Determination of vegetation cover fraction by inversion of a four-parameter model based on isoline parametrization.

A. Kallel, S. Le Hégarat-Mascleb, Catherine Ottle, Laurence Hubert-Moy

vailable online at www.sciencedirect.com
ScienceDirect
Remote Sensing of Environment 111 (2007) 553–566
Remote Sensing of Environment
www.elsevier.com/locate/rse

Determination of vegetation cover fraction by inversion of a four-parameter model based on isoline parametrization

Abdelaziz Kallel [a,*], Sylvie Le Hégarat-Mascle [b], Catherine Ottlé [c], Laurence Hubert-Moy [d]

[a] CETP/IPSL, 10–12 Avenue de l'Europe 78140, Vélizy, France
[b] IEF/AXIS, Université de Paris-Sud 91405, Orsay Cedex, France
[c] LSCE/IPSL, Centre d'Etudes de Saclay, Orme des Merisiers 91191, Gif-sur-Yvette, France
[d] COSTEL UMR CNRS 6554 LETG/IFR 90 CAREN, Université de Rennes 2, Place du recteur Henri Le Moal 35 043, Rennes Cedex, France

Received 6 December 2006; received in revised form 12 April 2007; accepted 14 April 2007

Abstract

This study focuses on the determination of the fraction of vegetation cover (fCover) based on the inversion of a four-parameter model combining the reflectances in the Red (R) and Near Infrared (NIR) domains. This model is semi-empirical since it is based on radiative transfer modeling, but requires parameter calibration related to SAIL simulations (Verhoef). As shown by Yoshioka et al., if the multiple soil/vegetation interactions are smaller than the first order ones then the fCover isolines can be approximated by straight lines in the (Red, Near Infrared) plane. Each isoline is completely defined by its slope α and its intersection point γ (with the soil line), that have been related to fCover using SAIL simulations and optimization either by the Simplex (local optimization) or the SCE–UA (global optimization) algorithms. The results are compared to classical vegetation indices for both simulated and actual data. The method shows an improvement in most of cases. Moreover, when using the SCE–UA algorithm, our approach proves its robustness relative to high noise level.

Keywords: Vegetation; fCover isoline; Parameter optimization; Vegetation indices

1. Introduction

Estimation of vegetation features from space is a great challenge for agronomist, hydrologist and meteorologist communities. For example, land cover during winter in agricultural regions strongly influences soil erosion processes and water quality (Dabney et al., 2001). Therefore, the identification and monitoring of vegetation cover constitutes a prior approach for the monitory of water resources. For such studies, the physical parameter used is the vegetation cover fraction (fCover). Now, the use of vegetation indices (Rondeaux et al., 1996) to estimate vegetation characteristics is very popular. They are empirical combinations between Visible (generally Red, R) and Near Infrared (NIR) reflectances that show good correlation with plant growth, vegetation cover, and biomass amount. Besides, theoretical methods based on radiative transfer model inversion allow vegetation feature retrieval like the Leaf Area Index (LAI), leaf area distribution, pigment concentration, or water content (Jacquemoud & Baret, 1990). Two kinds of inversion models are distinguished, those dealing only with one parameter (Baret et al., 1995; Kuusk, 1991a, 1995; Verstraete et al., 1990) and those dealing with many canopy parameters (Baret & Buis, 2007; Combal et al., 2002; Kimes et al., 2000). In this study, we propose to derive a semi-empirical method allowing the inversion of the fCover. Note that LAI is the vegetation biophysical parameter widely used by the empirical models described below. However, the canopy reflectances saturate for LAI values higher than values around 3 which makes the inversion too imprecise. Besides, in this study, the researched physical parameter is the fCover (used in the TNT-2 pollutant transfer mode (Durand et al., 2002)). Therefore, we propose to do the inversion directly in terms of fCover values, not using LAI as an intermediate variable (which would decrease the accuracy of the method).

In our study, the adding method (Cooper et al., 1982; van de Hulst, 1981) and the SAIL model (Verhoef, 1984, 1985) were combined to approximate the canopy reflectance, allowing its inversion. The well-known SAIL model, largely used in the

* Corresponding author. Tel.: +33 1 39 25 47 13; fax: +33 1 39 25 49 22.
E-mail address: abdelaziz.kallel@cetp.ipsl.fr (A. Kallel).

0034-4257/$ - see front matter © 2007 Elsevier Inc. All rights reserved.
doi:10.1016/j.rse.2007.04.006

remote sensing community, allows the calculation of the canopy Bidirectional Reflectance Distribution Function (BRDF). Based on the adding method approximation, a simple relationship between the R and NIR reflectances is derived in the case of homogeneous canopies (i.e. for a given field, vegetation density is assumed constant at any subscale). Then, as theoretically shown by Nilson (1971), assuming that the vegetation is a turbid medium, a one to one relationship exists between LAI and the gap fraction (allowing the incident flux to reach the soil) and then between LAI and fCover.

Having defined the direct model, the model inversion consists in determining the direct model input (fCover in our study) versus its observed outputs (reflectances). As a first step, vegetation isoline parameters are retrieved, that is similar to the approach of Yoshioka et al. (2002, 2003). In the case of non linear models, many inversion methods are based on Artificial Neural Network (ANN) simulations (Rumelhart et al., 1986) with applications such as function modeling, dynamic filtering, prediction and anomaly detection (Anderson, 1995). In our case, the main drawback is the important size of the learning or training data set required for ANN satisfying result (Anderson, 1995). Moreover, at the present time, no real mathematical justification has been provided for these approaches. In this study, our purpose is to assess the relationships between the fCover and the bidirectional reflectances in the R and NIR domains, having at our disposal a small database with noised observations and the direct radiative transfer model (SAIL and the adding method). Our problem is then reduced to the inversion of a four-parameter model for which classical optimization methods are sufficient.

In the following, we firstly present the theoretical bases (physical modeling and mathematical properties) of our semi-empirical inversion method: radiative transfer approximation, isoline set modeling. Secondly, we describe the proposed inversion method. Finally, the obtained results in terms of fCover are compared with those derived from classical vegetation indices.

2. Theoretical study

In this section, based on the SAIL model and the adding bidirectional reflectance approximations, we present an approximation of the fCover isoline as a segment of straight line. An isoline set parametrization is then empirically derived using SAIL simulations.

2.1. Vegetation isoline parametrization

The adding method (Cooper et al., 1982; van de Hulst, 1981) allows to model the radiative transfer between different vegetation layers and soil background as operators. Conversely, the SAIL model (Verhoef, 1984, 1985) allows the radiation flux modeling under a vegetation sublayer. In this subsection, we propose to simplify the bidirectional reflectance given by SAIL model using some adding method assumption.

Assuming the canopy is composed by a vegetation layer covering the soil, the flux reaching the top of the canopy is partly reflected without reaching the soil, and partly transmitted to the soil that will scatter it. Then, the flux is partially transmitted upward and partially reflected again to the soil, and so on (as illustrated on Fig. 1). The Adding method assumes that the total reflectance of canopy is the sum of the reflectance by the vegetation layer and the reflectance by the soil after a given number of interactions between the soil and the vegetation layer. The reflectance of the soil after a number $n \geq 1$ of soil–vegetation interactions is weakened due to the absorption by the leaves and the soil. The global reflectance operator of the canopy, noted $\mathbf{R}$ can then be modeled as a function of the reflectance and the transmittance operators of the vegetation layer and the reflectance operator of the soil:

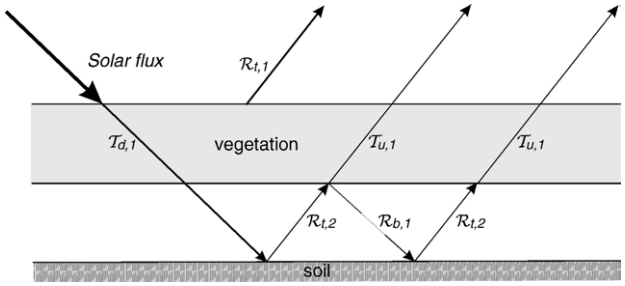

Fig. 1. Adding method operators: $\mathbf{T}_{d;1}$; $\mathbf{T}_{u;1}$ are respectively the downward and the upward vegetation layer transmittance operators, $\mathbf{R}_{t;1}$; $\mathbf{R}_{b;1}$ the top and the bottom vegetation layer reflectance operators and $\mathbf{R}_{t;2}$ the soil reflectance operator.

$$\mathbf{R}_t = \mathbf{R}_{t;1} + \mathbf{T}_{u;1} \circ (I - \mathbf{R}_{t;2} \circ \mathbf{R}_{b;1})^{-1} \circ \mathbf{R}_{t;2} \circ \mathbf{T}_{d;1}: \quad (1)$$

If the contribution of the multiple scattering between the vegetation and the soil is small relative to the single one (Yoshioka, 2004; Yoshioka et al., 2000a,b, 2002, 2003):

$$\mathbf{R}_t \subset \mathbf{R}_{t;1} + \mathbf{T}_{u;1} \circ \mathbf{R}_{t;2} \circ \mathbf{T}_{d;1}: \quad (2)$$

The SAIL model developed by Verhoef (1984, 1985) deals with the interactions between the radiation fluxes and the leaves. The bidirectional reflectance (R_{so}) is given by integrating the interactions between the fluxes and the vegetation over all kinds of leaves, knowing their geometric distribution and the depth of the vegetation layer. We assume that the canopy is composed of one vegetation layer covering the soil (Verhoef, 1985):

$$R_{so} = q_{so} + s_{ss} r_{so} s_{oo} + \frac{(s_{ss} r_{sd} + s_{sd} r_{dd} s_{do} + s_{sd} + s_{ss} r_{sd} q_{dd}) r_{do} s_{oo}}{1 - r_{dd} q_{dd}}; \quad (3)$$

where the $\rho_{..}$, $\tau_{..}$ terms are respectively the different components of vegetation reflectances and transmittances depending on the vegetation parameters (the leaf reflectance and transmittance (ρ, τ), LAI, leaf distribution) and the source and observation orientations, r_{so} the soil bidirectional reflectance, r_{do} the soil directional reflectance of hemispherical incidence, r_{sd} the soil hemispheric reflectance for direct incidence and r_{dd} the soil hemispherical reflectance for hemispherical incidence (Verhoef, 1985). Note that, τ_{ss} and τ_{oo} are two extinction terms depending only on the vegetation architecture. Physically these terms represent respectively the gap fractions in the direction of the source and the observation: when the source (respectively the observation) zenithal angle equals 0, τ_{ss} (respectively τ_{oo}) equals the gap fraction observed on the nadir direction (P_{gap}).

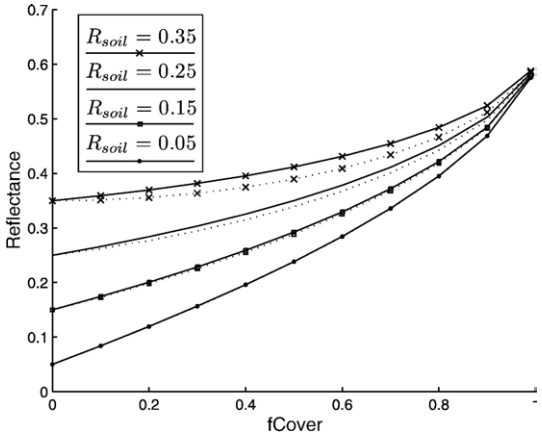

Fig. 2. Comparison between bidirectional reflectance of the canopy estimated by the SAIL model (continuous line) and its approximation (dashed line) (simulation parameters are given in Table 1).

Now, for our version of SAIL, the distribution of the leaf area is assumed ellipsoidal, with mean leaf inclination angle, noted *ALA*, that varies between 0 and 90°, from planophile vegetation to erectophile one (Campbell, 1990). Then, from the relationship of Nilson (1971) between LAI and P_{gap}, and having fCover equal to $1 - P_{gap}$:

$$\text{fCover} = 1 - \exp[-K_p(\text{ALA}):\text{LAI}]. \quad (4)$$

where K_p is the extinction factor that depends on and only on ALA. Eq. (4) is used in the following to link the canopy bidirectional reflectance (that depends on LAI in SAIL model) to the fCover.

Following the adding method approach (2), the SAIL model BRDF (3) is approximated at first order eliminating the terms depending on the soil reflectance r_{so}, r_{sd}, r_{do} and r_{dd} at high orders ($r_{..}^n$ for $n \geq 1$):

$$R_{so} \approx q_{so} + s_{ss} r_{so} s_{oo} + (s_{ss} r_{sd} + s_{sd} r_{dd} s_{do} + s_{sd} r_{do} s_{oo}).$$

In the Lambertian case, $r_{so} = r_{sd} = r_{do} = r_{dd} = R_{soil}$, and so:

$$R_{so} = q_{so} + (s_{ss} + s_{sd}) R_{soil} (s_{do} + s_{oo}). \quad (5)$$

Fig. 2 illustrates the good fitting of approximation (5) in the NIR case that is the more unfavorable case relative to visible one (Gausman et al., 1970; Jacquemoud & Baret, 1990) where in addition to NIR case τ_{sd} and τ_{do} are negligible compared to τ_{ss} and τ_{oo} (Suits, 1972):

$$R_{so} \approx q_{so} + s_{ss} R_{soil} s_{oo}. \quad (6)$$

The expressions (5) and (6) will be used as first order approximations of the reflectances in the NIR and R domains, respectively. In this study, we use the inputs listed in Table 1 that appear correct and for which change does not affect the interpretation of the results (Jacquemoud & Baret, 1990). Note that for simulations, the non simplified SAIL version is used.

Now, a couple of reflectance measurements for R and NIR spectral bands gives a point in the space (R, NIR). A set of points having the same fCover is called fCover isoline in the (R, NIR) space. The empirical linear relationship between the soil reflectances in R ($R_{soil,R}$) and NIR ($R_{soil,NIR}$) domains is called the soil line (Baret et al., 1989, 1993; Huete et al., 1984). It is defined through two parameters a_0 and b_0:

$$R_{soil;NIR} = a_0 R_{soil;R} + b_0; \quad (7)$$

From (5)–(7), for a homogeneous vegetation layer and for a given fCover, reflectances in R ($R_{so,R}$(fCover)) and NIR ($R_{so,NIR}$ (fCover)) are linearly linked:

$$R_{so;NIR}(\text{fCover}) = a(\text{fCover}) R_{so;R}(\text{fCover}) + b(\text{fCover}); \quad (8)$$

where:

$$a(\text{fCover}) = a \frac{(s_{ss} + s_{sd;NIR})(s_{do;NIR} + s_{oo})}{s_{ss} s_{oo}}; \quad (9)$$

$$b(\text{fCover}) = q_{so;NIR} - a(\text{fCover}) q_{so;R} + b_0 (s_{ss} + s_{sd;NIR}) \times (s_{do;NIR} + s_{oo}). \quad (10)$$

Whatever the source and the observation directions, $R_{so,R}(0)$, $R_{so,NIR}(0)$ are respectively equal to $R_{soil,R}$, $R_{soil,NIR}$, $\alpha(0) = a_0$ and $\beta(0) = b_0$.

Also, note that the property that the vegetation isolines are straight lines was also shown previously by (Huete, 1989; Yoshioka, 2004; Yoshioka et al., 2000a,b, 2002, 2003) and in (Yoshioka et al., 2000b) this property was extended to the heterogeneous canopy case.

Straight line parametrization from the SAIL parameters is complex and requires the knowledge of a priori information about the vegetation such as leaf distribution, pigment concentration, and water content. As an alternative, here we propose to search empirical relationships between the isoline parameters that will be used as a priori knowledge simplifying the model inversion.

2.2. Isoline set parametrization

A set of isolines is obtained by sampling the fCover. Fig. 3 shows a simulation of the SAIL model in (R, NIR) space corresponding to different values of fCover varying from 0 (bare soil) to 0.98 (very dense vegetation). Using the linear

Table 1
Simulation parameters and figure numbers where they are involved

Parameter	Vegetation layer			Leaf		Soil		Scene angles	
	ALA	fCover	Step	$(\rho, \tau)_{NIR}$	$(\rho, \tau)_R$	(a_0, b_0)	$[\min, \max]_R$	θ_s	(θ_o, φ_o)
Value	45°	[0, 0.98]	0.1	(0.47, 0.49)	(0.1, 0.09)	(1.1, 0.07)	[0.02, 0.32]	30°	(50°, 0°)
Figure number	2, 3, 6, 7	3, 7	3, 7	2, 3, 4, 6, 7	3, 4, 6, 7	3, 6, 7	3, 7	2, 3, 4, 6, 7	2, 3, 4, 6, 7

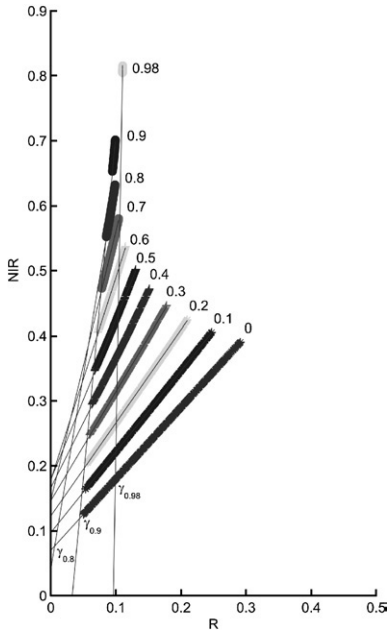

Fig. 3. SAIL simulation of fCover isoline set (simulation parameters are given in Table 1).

approximation for the fCover isolines, the average quadratic error remains lower than $5 \cdot 10^{-5}$. From Fig. 3, we note that the fCover isoline slope increases with vegetation density.

In the (R, NIR) space, the intersection of fCover isolines (8) and the soil line (7) is noted γ_{fCover} (Fig. 3)). γ_{fCover} is a function of α and β (Yoshioka et al., 2000b):

$$\gamma_{\mathrm{fCover}} = \left(-\frac{b-b_0}{a-a_0}; \frac{a_0 b - a b_0}{a_0 - a}\right) : \quad (11)$$

Lets change the coordinate plan such that X-axis becomes the soil line. The slope relating to this new coordinate plane is α':

$$a' = \frac{a-a_0}{1+a_0 a} : \quad (12)$$

Fig. 4 shows different simulations of SAIL for three ALA values. Fig. 4a shows the variations of α' versus fCover confirming the previously mentioned increase, particularly the relationship between α' and the fCover appears quasi-linear. Fig. 4b shows the variation of γ_a, X-coordinate of γ versus fCover: the curves are about linear, with a slope depending on ALA value.

Previous observations on Fig. 4 are formalized mathematically by:

$$\begin{aligned} a' &= g_1(1-(1-\mathrm{fCover})^{g_2}) + g_5; \\ \gamma_a &= g_3\,\mathrm{fCover} + g_4; \end{aligned} \quad (13)$$

where η_i, $i \in \{1, \ldots, 5\}$ are the isoline parameters. Taking into account the fact that when fCover = 0 the isoline coincides with the soil line,

$$g_5 = 0: \quad (14)$$

Note that for fCover negligible relative to one, $1-(1-\mathrm{fCover})^{\eta_2}$ is approximated by $(\eta_2 \mathrm{fCover})$ and so $\alpha'(\mathrm{fCover})$ is a linear function. For η_2 greater than one, the slope saturates for fCover close to 1, that is the case of erectophile vegetation. In Section 3, a derivation of $\xi = \{\eta_1, \eta_2, \eta_3, \eta_4\}$ from a learning data set will be proposed. Then using Eqs. (13) and (14), (α', γ_a) are obtained. In the following, we call 'direct model' the model that simulates (R, NIR) values knowing ξ. To inverse this model, the next subsection provides some mathematical properties.

2.3. Inverse problem: existence and unicity

For a homogeneous canopy, the inverse problem consists in deriving for each point of the (R, NIR) space the corresponding fCover value. It is shown below that a solution always exists and can be defined in a unique way.

Let $\mathcal{C}$ be the subpart of the (R, NIR) space formed by the envelope of the points corresponding to the ideal unnoisy spectral values in the (R, NIR) domain. We note $\mathcal{E}$ the subpart of (R, NIR) located between the soil line and any possible isoline. The isoline corresponding to a vegetation density fCover is called D_{fCover}. Fig. 5 shows, for an assumed soil line, the isoline set and the (R, NIR) subparts $\mathcal{C}$ and $\mathcal{E}$.

Let $M(x_M, y_M)$ be a point in the (R, NIR) plane. By definition of $\mathcal{E}$, $M \in \mathcal{E}$ if and only if $y_M \geq a_0 x_M + b_0$ and $\exists \mathrm{fCover}^s$ such as

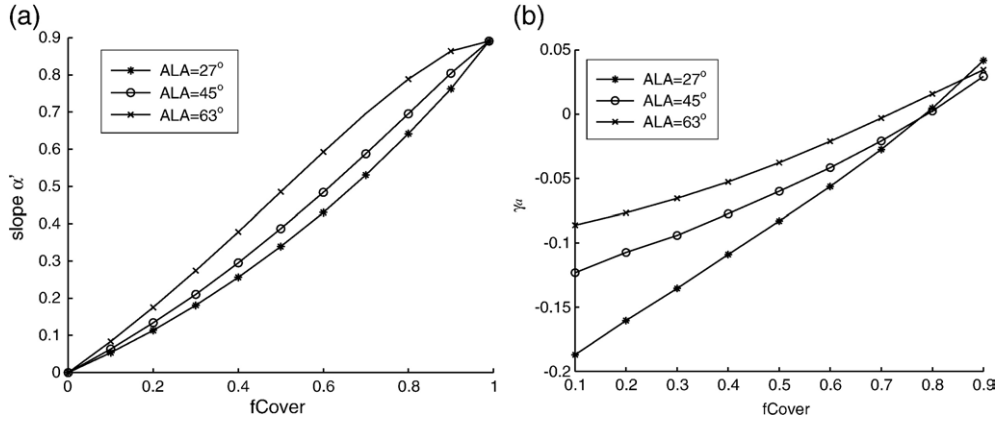

Fig. 4. SAIL simulations of planophile, extremophile and erectophile vegetation (simulation parameters are given in Table 1): (a) Isoline slope α' versus fCover, (b) γ_a (X-coordinate of γ) versus fCover.

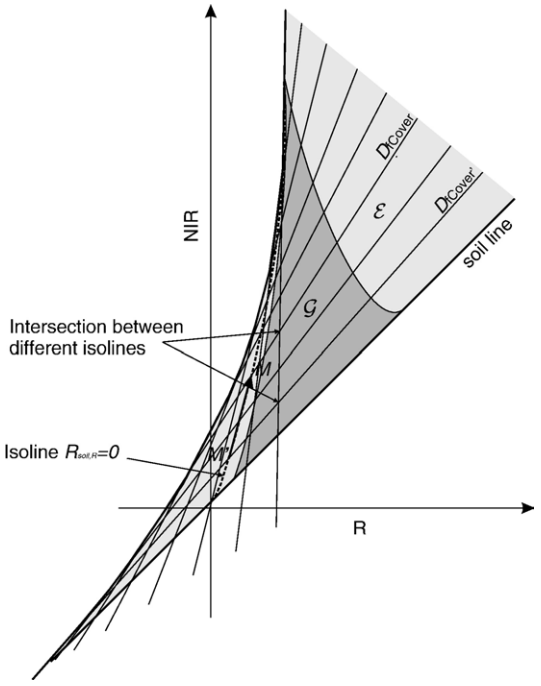

Fig. 5. Soil line, isoline set, G and E repartition in (R, NIR) space. Some intersections between isolines are shown in subpart G. D_{fCover} and $D_{fCover'}$ are two isolines, M and M' are two points respectively of D_{fCover} and $D_{fCover'}$, corresponding to null soil reflectance value in R band.

$y_M \le \alpha(\mathrm{fCover}^s)x_M + \beta(\mathrm{fCover}^s)$. Let g_M be the function defined by:

$$g_M(\mathrm{fCover}) = y_M - a(\mathrm{fCover})x_M - b(\mathrm{fCover}).$$

On the one hand, $g_M(\mathrm{fCover}^s) \le 0$, and on the other hand, $g_M(0) \ge 0$. The isoline parameters α' and γ_a are continuous functions of fCover on [0, 1], consequently α and β are also continuous functions of fCover on [0, 1]. Finally g_M being a linear function of α and β, g_M is a continuous function of fCover. Therefore, $\exists \mathrm{fCover}^*$ such as $g_M(\mathrm{fCover}^*)=0$ and therefore $y_M = \alpha_{\mathrm{fCover}^*} \cdot x_M - \beta_{\mathrm{fCover}^*}$. Then: $\forall M \in E$, $\exists \mathrm{fCover}^*$ such as $M \in D_{\mathrm{fCover}^*}$. Now, each edge point M in G corresponds to a vegetation density value fCover_M, then $M \in D_{\mathrm{fCover}_M}$. Since D_{fCover_M} belongs to E, then $M \in E$. Therefore, G is included in E.

From Fig. 5, several isolines can intersect at M. Calling S the set of fCover values whose isolines intersect at M, we now show that the actual M fCover value, called $\widetilde{\mathrm{fCover}}$, is the S lowest one:

$$\widetilde{\mathrm{fCover}} = \min_f \{ f = g_M(f) = 0 \}. \quad (15)$$

For this demonstration, it is sufficient to prove that any point in G corresponding to vegetation density fCover is higher (belonging to the mid-high plane) than any $D_{\mathrm{fCover}'}$ such as $\mathrm{fCover}' < \mathrm{fCover}$. We have to show that each actual point of the D_{fCover} line is higher than $D_{\mathrm{fCover}'}$. As the parameter α is an increasing function of fCover (Eq. (9) and Fig. 4), the slope of D_{fCover} is greater than the slope of $D_{\mathrm{fCover}'}$, and it is sufficient to show that the point of D_{fCover} with the lowest x-coordinate is above $D_{\mathrm{fCover}'}$. Since this point corresponds to the lower value of the R soil reflectance that is higher than 0, it is sufficient to show this property for a point corresponding to a null soil reflectance value in R band (called $M(r, nir)$). Let $M'(r', nir')$ be the point of $D_{\mathrm{fCover}'}$ with null value of soil reflectance in R band (Fig. 5). In order to show that M is above $D_{\mathrm{fCover}'}$, it is sufficient to show that the slope of the line $(M'M)$, i.e. $\frac{nir - nir'}{r - r'}$, is higher than the slope of $D_{\mathrm{fCover}'}$, i.e. $\alpha_{\mathrm{fCover}'}$. We have then to point out that:

$$\frac{R_{so;NIR}(\mathrm{fCover}) - R_{so;NIR}(\mathrm{fCover}')}{R_{so;R}(\mathrm{fCover}) - R_{so;R}(\mathrm{fCover}')} > \alpha_{\mathrm{fCover}'}; \quad (16)$$

Let $s = \left(\frac{\partial R_{so;NIR}}{\partial \mathrm{fCover}} \Big/ \frac{\partial R_{so;R}}{\partial \mathrm{fCover}} \right)^{-1}$, it is derived by dividing Eq. (16) left member numerator and denominator by $\mathrm{fCover} - \mathrm{fCover}'$ and making fCover' converge towards fCover. s is the slope of variation of M versus fCover whereas α is the slope of variation of M versus the soil reflectance. Assume that $s > \alpha$:

$$s(\mathrm{fCover}) > \alpha_{\mathrm{fCover}} \Leftrightarrow \frac{\partial R_{so;NIR}(\mathrm{fCover})}{\partial \mathrm{fCover}} > \alpha_{\mathrm{fCover}} \frac{\partial R_{so;R}(\mathrm{fCover})}{\partial \mathrm{fCover}};$$
$$\int_{\mathrm{fCover}'}^{\mathrm{fCover}} \frac{\partial R_{so;NIR}(t)}{\partial t}\,dt > \alpha_{\mathrm{fCover}'} \int_{\mathrm{fCover}'}^{\mathrm{fCover}} \frac{\partial R_{so;R}(t)}{\partial t}\,dt;$$
$$\int_{\mathrm{fCover}'}^{\mathrm{fCover}} \frac{\partial R_{so;NIR}(t)}{\partial t}\,dt > \alpha_{\mathrm{fCover}'} \int_{\mathrm{fCover}'}^{\mathrm{fCover}} \frac{\partial R_{so;R}(t)}{\partial t}\,dt;$$
$$\frac{R_{so;NIR}(\mathrm{fCover}) - R_{so;NIR}(\mathrm{fCover}')}{R_{so;R}(\mathrm{fCover}) - R_{so;R}(\mathrm{fCover}')} > \alpha_{\mathrm{fCover}'}.$$

So, to show Eq. (16), it is sufficient to show that $s > \alpha$.

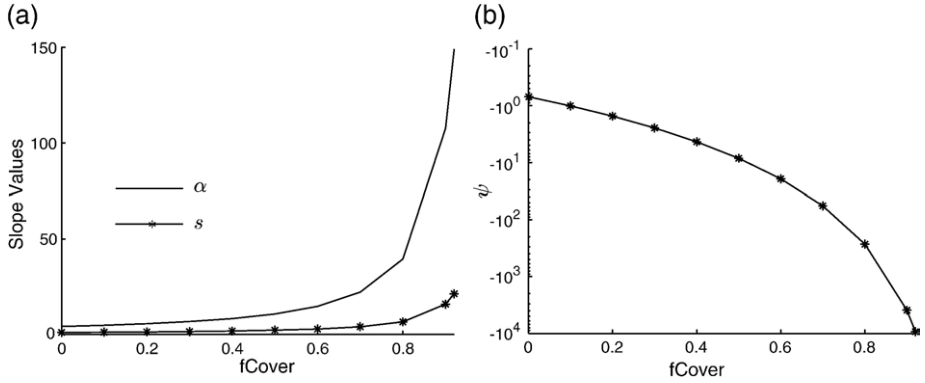

Fig. 6. (a) Variation of s and α versus fCover, (b) Variation of ψ versus fCover. The simulation parameters are presented in Table 1.

Using the SAIL model, we find as illustrated on Fig. 6a that s is always larger than α. Moreover, due to the saturation of the Red reflectance, the difference increases while increasing fCover. Roughly, this means that, when the soil reflectance is equal to 0, the variation of the reflectances in the (R, NIR) plane versus the fCover is higher than their variation versus the soil reflectance.

We now show that the cardinal of S is lower than 2. For this purpose, it is sufficient to show that the intersection between three isolines is the empty set. According to Appendix A, it is sufficient to show that:

$$\frac{\partial^2 b}{\partial \mathrm{fCover}^2}\frac{\partial a}{\partial \mathrm{fCover}} - \frac{\partial b}{\partial \mathrm{fCover}}\frac{\partial^2 a}{\partial \mathrm{fCover}^2} \neq 0: \quad (17)$$

Fig. 6b presents the variation of ψ versus fCover. ψ is a decreasing function of fCover with $\psi(0) \neq 0$. Thus, Eq. (17) is true and therefore in each actual point in (R, NIR) intersects at maximum two different isolines. This property will be used in Section 3 to optimize the derivation of the fCover based on the isoline parametrization.

3. Method implementation

The previous section presented the ideal case where data were unnoised and model is exact. Now, for actual inversion, $\tilde{G}$ (observed G) and $\hat{E}$ (estimated E) are introduced: $\tilde{G} \subset G$ and $\hat{E} \subset E$ except at the borders of the domains. The previous properties are still true provided that $\tilde{G} \cap \hat{E}$.

This section first deals with the estimation of ξ using a learning data set and secondly with the inversion method.

3.1. Parameter estimation

Assuming that the soil line parameters are known, the remaining isoline parameters (i.e. ξ set) are estimated using a learning data set, formed by N_{learn} points M_i, $i \in \{1, ..., N_{\mathrm{learn}}\}$, in G, for which the fCover value is known. The optimization of ξ is done according to the Root Mean Square Error (RMSE) minimizing criterion and the fCover_i isolines. For this, we define the distance between M_i and the associated fCover_i isoline as equal to $\frac{g_i - \partial \mathrm{fCover}_i}{1 + a_{\mathrm{fCover}_i}^2}$. Then noting $g_i = g_{M_i}$ and $\alpha_i = \alpha_{\mathrm{fCover}_i}$, $L(.)$ the functional to minimize,

$$L(\xi) = \sum_{i=1}^{N_{\mathrm{learn}}} \frac{g_i - \mathrm{fCover}_i(\xi)}{1 + a_i^2}^2; \quad (18)$$

The use of an optimization technique is justified since:

- the presence of both polynomial and exponential terms in $L(\xi)$ makes the analytical inversion of L impracticable;
- approximately, the domain of variation of $(\eta_1, \eta_2, \eta_3, \eta_4)$ is $[0.2, 1.2] \times [0.9, 1.5] \times [0.0, 0.55] \times [-0.4, 0]$, and the aimed precisions for these parameters are respectively 10^{-2}, 10^{-3}, 10^{-3} and 10^{-3}. Therefore, an exhaustive search corresponds to a number of configurations to test of about 1.32×10^{10}.

Distinction between optimization methods occurs generally in terms of deterministic or stochastic features. Deterministic approaches are efficient for linear problems or convex functions presenting one and only one extremum. In the case of local extrema, the optimization result depends on the initialization making not sure the convergence towards the global optimum. For such cases, only stochastic approaches can reach the global optimum, even if mathematical convergence has been proved only for few algorithms (e.g. simulated annealing). In other cases, heuristics allow the obtention of 'good' solutions without warranting the global optimum. In our case, the solution space of L is not convex and simulation tests showed the existence of many local optima. We compare the result of a deterministic method the Simplex (Dantzig et al., 1955; Nelder & Mead, 1965), and a heuristic, the Shuffled complex algorithm (SCE–UA) (Duan et al., 1992; Sorooshian et al., 1992) which uses many Simplex simultaneously and in competition.

The Simplex has been developed by Dantzig et al. (1955) for numerical resolution of linear problems and extended to the non linear case by Nelder and Mead (1965), in order to reach the global optimum in convex spaces. Assuming the solution space is of dimension N_s, the researched optimum O^* will be surrounded by a polytope P of $N_s + 1$ vertices (corners), by displacing these vertices until being sure that O^* is inside P and that the size of P is in agreement with required precision on O^*. The method evolution is done by the Algorithm 1.

In order to overcome the local minima, SCE–UA is a heuristical technique using many Simplex simultaneously. SCE–UA uses p subsets called complex of $2N + 1$ points (in our application, we choose $p = 12$). Each complex evolves (independently to the others) during a few number of iterations. Following a probabilistic law (function of the cost), a set of points $(N_s + 1)$ is extracted that evolves as a Simplex during $\sharp it$ iterations (in our case $\sharp it = 2N_s + 1$). After evolution, the complexes are merged: all elements are sorted before redistribution into new complexes, allowing the local minima to 'go out'. The processes (complex evolution, complex merging and complex distribution) are repeated until convergence.

Algorithm 1. Simplex Method

1. Selection of $N_s + 1$ vertices $\{v_1, v_2, ..., v_{N_s+1}\}$ as initialization of the Simplex;
2. Sorting the vertices according to their cost $ct(v_1) \leq ct(v_2) \leq ... \leq ct(v_{N_s+1})$;
3. Computation of the centroid of the N_s lowest cost vertices $g = \frac{1}{N_s}\sum_{i=1}^{N_s} v_i$;
4. Reflection of the worse vertex through the centroid $r = g - v_{N_s+1}$. If the cost is decreasing: $ct(r) \leq ct(v_{N_s+1})$, do the update: $v_{N_s+1} \leftarrow r$, else go to step 6;
5. Expending of the reflection by factor 2: $e = g - 2v_{N_s+1}$. If the cost decreases: $ct(e) \leq ct(r)$, do the update: $v_{N_s+1} \leftarrow e$, go to step 8;
6. Contraction: $t = \frac{g + v_{N_s+1}}{2}$. If $ct(t) \leq ct(v_{N_s+1})$, do the update: $v_{N_s+1} \leftarrow t$, go to step 8;
7. Shrinking the whole Simplex: update the vertices $\{v_i, i \in \{2, ..., N_s + 1\}\}$; by moving them halfway between their location and v_1 : $v_i = \frac{v_i + v_1}{2}$
8. Test of convergence: based on the 'size' of the Simplex (distance between vertices).

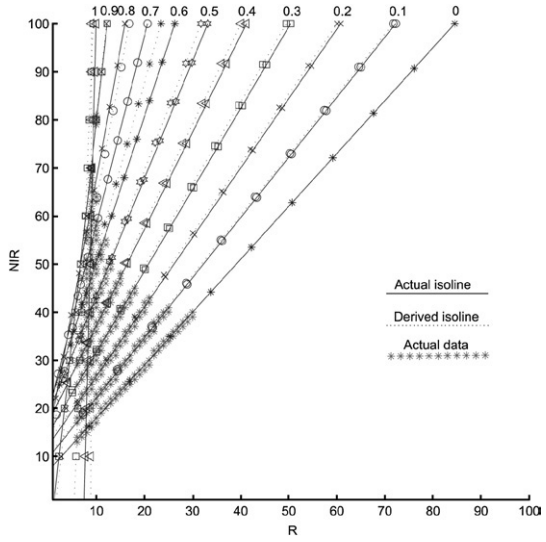

Fig. 7. Sets of isolines actual and derived by the SCE–UA method (the simulation parameters are presented in Table 1).

Fig. 7 shows both the actual set of fCover isolines and those derived by the SCE–UA method. For higher fCover values, the isoline estimation is the less accurate due to the added complexity for dense vegetation (saturation in the red spectral domain).

3.2. Model inversion

Having defined the set of isolines, the model inversion attributes to each point M of $\tilde{\iota}$ a vegetation density value fCover corresponding to the first fCo$\tilde{}$ver which makes g_M null (15). From Section 2.3 and as illustrated by Fig. 8, g_M can have either one or two zeros. As $g_M(0) \geq 0$ (all points are above the soil line), then fCo$\tilde{}$ver is before the unique interval such as g_M is negative: $\tilde{f} \in [f_1, f_2]$ with $0 = f_1 < f_2 \leq 1$, $g_M(f_1) \geq 0$ and $g_M(f_2) \leq 0$. In the case of one zero, we can choose $f_2 = 1$. Otherwise, an ad hoc initialization of f_2 in the interval [0, 1] has to be performed. Then, $\tilde{f}$ is derived using a dichotomic search between $[f_1, f_2]$ with an accuracy of about 10^{-4} (in our case).

Note that, because of noise and the model imperfection, the two unexpected situations may be encountered:

- $g_M(0) > 0$: we set fCo$\tilde{}$ver = 0;
- $g_M(f) < 0 \ \forall f \in [0, 1]$: we set fC$\tilde{o}$ver = 1.

4. Validation data

In this section the proposed method is compared to the fCover estimation with the other widely used vegetation indices (*VI*), both considering simulated and actual data. In the last decades, many vegetation indices combining the R and NIR spectral bands have been developed (Rondeaux et al., 1996). Those used here are listed in Table 2. Experimental and theoretical studies showed the correlation between them and vegetation features such as LAI, fCover and vegetation health.

Now, according to Clevers (1989) and Baret and Guyot (1991), a vegetation index is linked to LAI by:

$$VI = VI_\infty + (VI_s - VI_\infty)\exp(-K_{VI} LAI);$$

with VI_s and VI_∞ the vegetation indices respectively for bare soil (LAI= 0) and very dense vegetation (LAI=∞). From Eq. (4) and the previous equation, the relationship between fCover and VI is (Baret et al., 1995):

$$fCover = 1 - \frac{VI - VI_\infty}{VI_s - VI_\infty}^{\frac{K_p}{K_{VI}}}; \quad (19)$$

Practically, VI_s and VI_∞ are the average values of the vegetation indices over the points respectively of the bare soil and with fCover$\lesssim$ 1. The factor $\frac{K_p}{K_{VI}}$ is derived as the value minimizing the estimation RMSE (18) over the interval [0.5, 5] with a step equal to 10^{-3}.

4.1. Simulated data

The simulated data have been derived using both the SAIL and PROSPECT models (Fourty & Baret, 1997, 1998; Jacquemoud & Baret, 1990). Varying the soil and the vegetation features, many simulations have been carried out. Such simulations allow both the intercomparison between the fCover retrieval methods and the study of our model sensitivity to different parameter variation and noise.

The PROSPECT model is a radiative transfer model allowing the derivation of the hemispherical reflectance and transmittance of leaves from the knowledge of different matter concentrations and features which absorb the radiation. In the Visible domain, absorption is mainly due to pigment concentration (chlorophyll $a + b$) C_{a+b}. In the NIR domain, the absorption is lower, and it is due to the mesophyll leaf structure, in particular the number of sublayers, N. The SAIL input parameters are the leaf reflectance and transmittance simulated by PROSPECT, the vegetation density (fCover), leaf area distribution (ALA), the sun and observation geometry: sun zenithal angle (θ_s), observation zenithal and azimuthal angles (θ_o, φ_o), hot spot parameters (h_s) (Andrieu et al., 1997; Kuusk, 1985, 1991b), and the soil reflectances ($R_{soil,R}$, $R_{soil,NIR}$) that are entirely determined by Red soil reflectance variation $[\min_{R_{so,R}}, \max_{R_{so,R}}]$ and the soil line equation (a_0, b_0). Following Huete et al. (1984) and Baret et al. (1993), the soil type

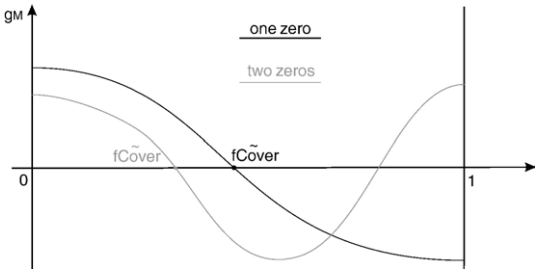

Fig. 8. g_M versus fCover for the two cases: 1 and 2 zero function.

Table 2
Vegetation indices

Index	Abbreviation	Formulation
Perpendicular vegetation index (Richardson & Wiegand, 1977)	PVI	$\frac{r_{NIR} - a_0 r_R - b_0}{\sqrt{a_0^2 + 1}}$
Weighted infrared–red vegetation index (Clevers, 1989)	WDVI	$r_{NIR} - a_0 r_R$
Ratio vegetation index (Pearson & Miller, 1972)	RVI	$\frac{r_{NIR}}{r_R}$
Normalized difference vegetation index (Rouse et al., 1974)	NDVI	$\frac{r_{NIR} - r_R}{r_{NIR} + r_R}$
Soil-adjusted vegetation index (Huete, 1988)	SAVI	$(1 + L)\frac{r_{NIR} + r_R}{r_{NIR} + r_R + L}; L = 0.5$
Transformed soil adjusted vegetation index (Baret & Guyot, 1991; Baret et al., 1989)	TSAVI	$\frac{a_0(r_{NIR} - a_0 r_R - b_0)}{a_0 r_{NIR} + r_R - a_0 b_0 + X(1 + a_0^2)}; X = 0.08$
Modified soil adjusted vegetation index (Qi et al., 1994)	MSAVI	$\frac{1}{2}\left[2r_R + 1 - \sqrt{(2r_R + 1)^2 - 8(r_R - r_{NIR})}\right]$

variability is simulated by an additive noise (ϵ_{so}) on the soil line equation:

$$R_{soil;NIR} = a_0 R_{soil;R} + b_0 + s_{so}$$

In this section, for all experiences, (a_0, b_0) and [$\min_{R_{so,R}}$, $\max_{R_{so,R}}$] are assumed fixed and equal respectively to (1.1, 0.07) and [0.02, 0.32].

Table 3 shows the set of simulations which will be used to compare the performance of the proposed method to classical vegetation indices and evaluate the robustness of the method to parameter inaccuracy (spatial and/or noise). The three first sets of simulations (scenarii 1 to 3) test the impact of LAD variation, the scenarii 4, 5 and 6 deal with the leaf features, the scenario 7 tests the effect of the hot spot and finally the scenario 8 tests both the effect of noise inaccuracy over all parameters and on the hot spot effect. Table 4 presents the RMSE obtained considering the different tests and the different methods. Tests 1, 2 and 3 show that the variation of ALA (planophile, extremophile and erectophile) of the vegetation has small influence on the estimation performance. We also see that MSAVI and TSAVI give accurate results for respectively small and large ALA values. Test 4, which corresponds to the presence of more senescent vegetation, shows that the variation of vegetation features does not have important effects on the performance of the method. Tests 5 and 6 point out that the uncertainties over the pigment concentration affect more the results than the uncertainties over mesophyll leaf structure. Test 7 shows that the hot spot effect (when the source and the observation have the same solid angle), even in the case of uncertainty over its value,

Table 3
Set of simulations used to evaluate the performance of the method

Test	C_{a+b}		N		h_S		fCover	ALA	θ_s	θ_o	φ_α
	[1]M	[2]Sdv	M	Sdv	M	Sdv	Sdv				
1	30	0	1.5	0	0.3	0	0	45°	30°	50°	0°
2	30	0	1.5	0	0.3	0	0	27°	30°	50°	0°
3	30	0	1.5	0	0.3	0	0	63°	30°	50°	0°
4	20	0	2	0	0.3	0	0	45°	30°	50°	0°
5	30	6	1.5	0	0.3	0	0	45°	30°	50°	0°
6	30	0	1.7	0.3	0.3	0	0	45°	30°	50°	0°
7	30	0	1.5	0	0.3	0.05	0	45°	30°	30°	0°
8	30	6	1.7	0.3	0.3	0.05	0.04	45°	30°	30°	0°

[a]Mean value.
[b]Standard deviation.
The isoline set is obtained varying fCover from 0 to 0.98 (sample step equal to 0.1). When 'Sdv = 0' (by default for the 4 last parameters), the parameter value is given in first (or unique) column, else it is a random value generated following a normal distribution $N(M; Sdv)$. Grey cells point out differences with first test configuration.

Table 4
RMSE obtained using different methods, in the different cases of test, and for training (top value, 100 points) and validation sets (bottom value, 120 points)

Test number	Simplex	SCE–UA	PVI	WDVI	RVI	NDVI	SAVI	TSAVI	MSAVI
1	0.017	0.011	0.044	0.044	0.071	0.068	0.028	0.026	0.02
	0.017	0.012	0.044	0.044	0.081	0.079	0.028	0.028	0.019
2	0.017	0.017	0.039	0.039	0.068	0.082	0.027	0.026	0.02
	0.018	0.018	0.034	0.034	0.076	0.084	0.025	0.025	0.02
3	0.022	0.018	0.039	0.039	0.077	0.071	0.024	0.018	0.03
	0.021	0.018	0.042	0.042	0.069	0.063	0.024	0.018	0.033
4	0.02	0.019	0.039	0.039	0.075	0.091	0.025	0.02	0.028
	0.019	0.016	0.043	0.043	0.062	0.081	0.023	0.017	0.027
5	0.042	0.043	0.047	0.047	0.135	0.128	0.052	0.067	0.054
	0.04	0.035	0.045	0.045	0.122	0.117	0.044	0.058	0.05
6	0.02	0.02	0.047	0.047	0.101	0.086	0.025	0.026	0.024
	0.022	0.022	0.044	0.044	0.097	0.082	0.027	0.03	0.025
7	0.017	0.008	0.038	0.038	0.117	0.089	0.022	0.033	0.015
	0.017	0.008	0.036	0.036	0.106	0.085	0.019	0.029	0.012
8	0.061	0.057	0.068	0.068	0.1	0.099	0.059	0.064	0.062
	0.049	0.052	0.064	0.064	0.103	0.104	0.054	0.061	0.057

Per line, the dark grey cell shows the best result, and the light grey one the second best result.

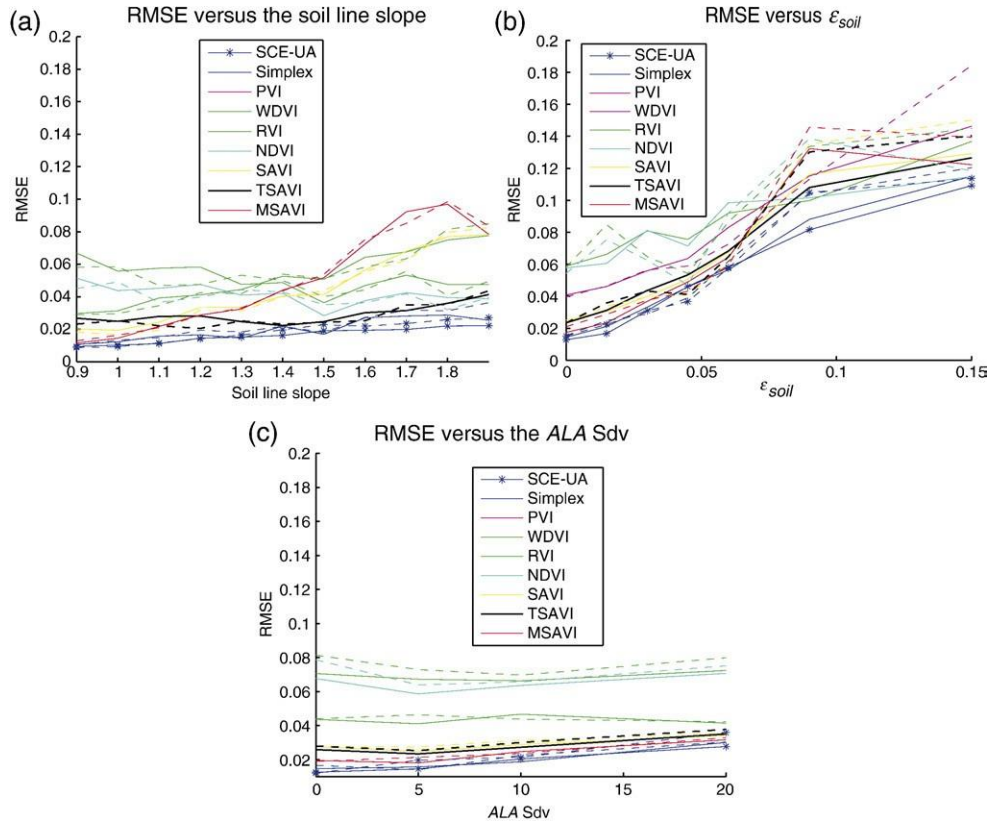

Fig. 9. Robustness tests: fCover estimation variation versus canopy parameters. The solid (resp. dashed) curves correspond to the learning (resp. validation) set.

has no significant impact on the fCover estimation accuracy. Test 8 shows the results assuming an accentuation of the hot spot effect and both uncertainties over the soil line, concentration of chlorophyll, mesophyll leaf structure and hot spot. The relatively large error is mainly due to the strong influence of the C_{a+b} concentration inaccuracy (as in test 5), and the influence of the mesophyll (N) variability (as in test 6).

About the respective performance of the different vegetation indices, it is shown that SCE–UA and Simplex perform better. Moreover, due to the non convexity of $L(\xi)$ over the solution space, SCE–UA gives often more accurate results than the Simplex. In our application, the Simplex algorithm was run many times to lead to sufficiently accurate results. Only considering classical vegetation indices (Table 2), we note that for unnoised data (tests 1 to 4), TSAVI performs often better, whereas MSAVI and SAVI are more robust to noised data (tests 5 to 8). The fact that PVI and WDVI give the same result is consistent since they are linearly dependent. Finally, note that there is no significant difference between training and validation sets. This result is very satisfying and means that using a set of 100 elements for training, as we did, is statistically sufficient.

Supplementary simulations are shown in Fig. 9 which presents three robustness tests in case of: variation of soil line slope, noise added on soil line and ALA. Fig. 9a shows the robustness to the slope variation. SCE–UA and Simplex show a small degradation of performance versus the slope value. Since

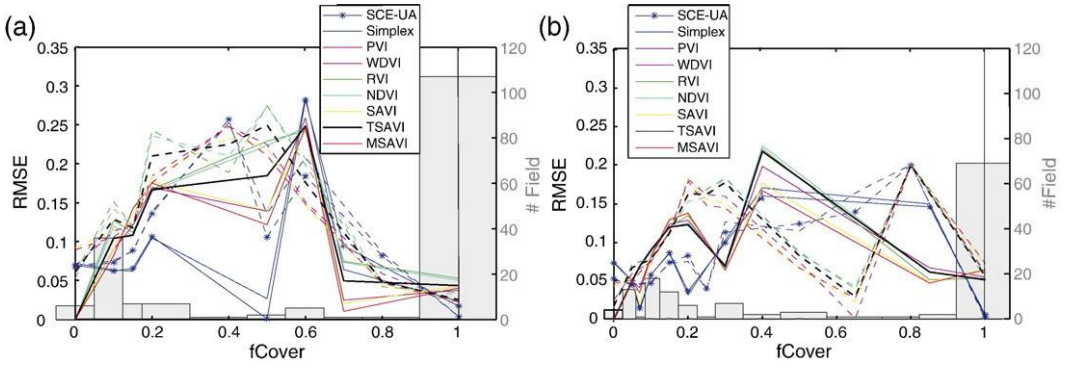

Fig. 10. Ground fCover distribution (grey rectangles) and RMSE distributions versus fCover: (a) 2003, (b) 2006. The solid (resp. dashed) curves correspond to the learning (resp. validation) set.

it takes into account the effective soil line, TSAVI is the more robust, conversely to SAVI and MSAVI whose performance decreases dramatically versus the slope value. Fig. 9b shows that the increase of the soil line noise affects quasi-linearly the fCover estimation performance. Fig. 9c shows that the increase of ALA variation domain does not affect significantly the results. In summary, for all these tests the developed method gives accurate estimation results, better that those obtained using any classical vegetation index.

4.2. Actual data

Now, in order to validate the proposed method, both remote sensed data and reference field data (ground truth) measurements acquired simultaneously over the Yar watershed (61 km^2), located in a fairly intensive farming area in northern Brittany in France has been carried out for several years (Corgne et al., 2002).

4.2.1. Ground truth data

In 2003 and 2006, ground truth measurements corresponding respectively to 244 and 155 fields have been acquired. The field average area is 1 ha. For each visited field, an estimation of the fCover was derived with a 5% precision for low fCover values (fCover ≤ 25%) and a 10% accuracy for high fCover value (fCover ≥ 25%). On Fig. 10, the gray rectangles show the distribution of fCover ground measurements. Since the majority of fields are covered in winter, we observe a pick for fCover = 1. Fields with mean vegetation are few, since the leaseholders are either respecting law (winter coverage) or not respecting it, but rarely respecting it only partially.

The actual soil line parameters were determined from the analysis of six soil samples collected from six agricultural fields. Having dried the samples, they were wetted again progressively, measuring the soil reflectance (with a spectrometer) to plot the NIR reflectance versus the R one. Table 5 shows the soil line parameters obtained from each sample. For the following of our study, the slope a_0 is set equal to the mean slope, and the intercept b_0 equal to zero.

4.2.2. Remote sensing data

Two satellite images have been acquired over the Yar basin. The first one is a high resolution SPOT 5 image (pixel size equal to 10 m × 10 m, 4 frequency bands: Green (500−590 nm), Red (610−680 nm), NIR (780−890 nm) and Mean Infrared (1580−1750 nm)) acquired on 01/24/2003, and the second one a very-high resolution Quickbird image (pixel 2.8 m × 2.8 m, 4 frequency bands Blue (450−520 nm), Green (520−600 nm), Red (630−690 nm) and NIR (760−900 nm)) acquired on 03/22/2006.

Table 5
Soil line parameters: for samples (1 to 6) and the used values in the following

Sample	1	2	3	4	5	6	Used values	RMSE
a_0	1.7	1.67	1.68	1.62	1.56	1.48	1.62	0.085
b_0	0.008	0.015	0.005	−0.02	−0.011	−0.02	0	0.016

The RMSE are calculated between the samples and the used values.

Now, for each frequency band (*fb*) and in the absence of atmospherical corrections, the data measurement is the reflectance top of atmosphere (*TOA*), noted R_{fb}^{TOA}, which is a linear function of the reflectance top of canopy (*TOC*), noted R_{fb}^{TOC} (Tanré et al., 1990; Vermote et al., 1997):

$$R_{fb}^{TOC} = A_{fb} R_{fb}^{TOA} + B_{fb}. \quad (20)$$

In our study, R_{fb}^{TOC} values are required. To derive the couple (A_{fb}, B_{fb}) for each image and for R and NIR bands, the following processing was performed:

- *Spatial low frequency filtering (field level):* since the ground truth measurement is equal to the more frequent vegetation density on the considered field, a remote sensing value at field scale is derived accordingly as the mode (more frequent value) of the distribution of the pixel values over the considered field.
- *Determination of the TOA soil line:* using TOA reflectances measurement, the soil line derived from these measurements is different from the ground truth soil line (computed in Section 4.2.1) which corresponds to TOC observations. Due to the insufficient range of ground truth points, (a_0^{TOA}, b_0^{TOA}) is derived as follows: a linear regression between the R and NIR values is made for the points $(M_i^l(R_i^l, NIR_i^l))_{i=\{1,\ldots,N_l\}}$ corresponding to the lower R values for each NIR value in the (R, NIR) space, and the points $(M_i^p(R_i^p, NIR_i^p))_{i=\{1,\ldots,N_p\}}$ corresponding to the fields with null fCover value:

$$(a_0^{TOA}; b_0^{TOA}) = \underset{a;b}{\operatorname{argmin}} \left\{ \frac{1}{N_l} \sum_{i=1}^{N_l} \frac{(NIR_i^l - aR_i^l - b)^2}{a^2+1} + \frac{1}{N_p} \sum_{i=1}^{N_p} \frac{(NIR_i^p - aR_i^p - b)^2}{a^2+1} \right\}.$$

  Note that the normalization by $N_l \simeq 10^3$ and $N_p \simeq 10$ gives the same weight to the two sets of points respectively derived from ground truth and image histogram analysis.
- *NIR reflectance calibration:* NIR channel calibration was done from a priori knowledge about specific targets: water and forest. On the one hand, the water reflectance (R^w) in NIR band is assumed null. Therefore from Eq. (20):

$$A_{NIR} R_{NIR}^{TOA;w} + B_{NIR} = 0. \quad (21)$$

On the other hand, one can assume that the dense coniferous forests keep a constant bidirectional reflectance (R^f) all along the year and are Lambertian reflectors (Holben & Kimes, 1986). Then assuming that the atmospherical effects are negligible in summer ($R^{TOA} \approx R^{TOC}$), the forest reflectances have been estimated from an additional summer image used to constraint the winter NIR TOC reflectances (20):

$$A_{NIR} R^{TOA;f} + B_{NIR} = R^{TOC;f}. \quad (22)$$

Eqs. (21) and (22) give: $A_{NIR} = \frac{R_{NIR}^{TOC;f}}{R_{NIR}^{TOA;f} - R_{NIR}^{TOA;w}}$ and $B_{NIR} = -\frac{R_{NIR}^{TOA;w} R_{NIR}^{TOC;f}}{R_{NIR}^{TOA;f} - R_{NIR}^{TOA;w}}$:

- *R reflectance calibration:* after NIR calibration, linking the TOA soil line to the TOC one, the R reflectance calibration is:

$$R^{\mathrm{TOC}}_{\mathrm{soil;R}} = A_{\mathrm{R}} R^{\mathrm{TOA}}_{\mathrm{soil;R}} + B_{\mathrm{R}};$$

where $A_{\mathrm{R}} = \frac{A_{\mathrm{NIR}} a_0^{\mathrm{TOA}}}{a_0}$ and $B_{\mathrm{R}} = \frac{A_{\mathrm{NIR}} b_0^{\mathrm{TOA}} + B_{\mathrm{NIR}} - b_0}{a_0}$:

Table 6 shows the fCover estimation RMSE using the developed method and classical vegetation indices. Fig. 10 shows the distribution of the RMSE versus fCover superposed to the fCover histogram. In general, the obtained RMSE are large. Firstly, a part of this error can be explained by the ground measurement 'weak' accuracy especially for dense fields (ground fCover± 5%). Secondly, the diversity of biophysical features, especially the senescent vegetation, influencing the radiative properties. Less concentration of chlorophyll (C_{a+b}) leads to the increase of the red vegetation reflectance. Conversely, in the NIR domain, the senescent leaf internal structure is increasing the equivalent number layers (N), the leaf absorption and decreasing the whole vegetation reflectance. Senescent vegetation is found both for fields having low cover only due to the remainder of crop (Fig. 10 shows a relatively high RMSE for low fCover) and for covered meadow fields affected by cattle trod on and grazing. Due to this latter case, in the (R, NIR) space, the isolines corresponding to the fCover values close to 1 are spread out abnormally in comparison with SAIL simulation (2). Now, considering the more significant points of (Fig. 10) curves, i.e. modes of the fCover histograms: values about 0.1 and 1, SCE–UA and Simplex RMSE are lower than the classical vegetation index ones.

A more surprising observation is the closeness of the results (Simplex, SCE–UA, classical vegetation indices) since the soil line slope is rather high, and according to the simulations (cf. Fig. 9a), the indices which do not take into account the soil line provide less accurate results. We explain this absence of soil line sensitivity by the fact that in winter, the soil is very wet (almost saturated) due to the abundant rains, therefore the surface reflectance spatial variability is too low to let appear the soil line dependence.

Finally, although a larger ground truth data set is available for 2003, the fCover estimation results of 2006 are more consistent between the learning and validation set results. This can be explained by (i) the fact that, the Quickbird image is a high resolution image allowing the extraction of 'pure' pixels by elimination of the field edges and lanes, and (ii) the fact that, for the Quickbird image the number of pixels per field is almost 13 times greater than for the SPOT 5 image making the statistical estimation of modal value more accurate.

Table 6
Actual data RMSE for different methods for training (top value) and validation sets (bottom value) having the same number of points (the half of the total number of fields)

Test number	Simplex	SCE–UA	PVI	WDVI	RVI	NDVI	SAVI	TSAVI	MSAVI
SPOT5	0.052	0.05	0.069	0.069	0.086	0.082	0.072	0.075	0.069
	0.078	0.074	0.093	0.093	0.116	0.112	0.094	0.102	0.09
Quickbird	0.06	0.059	0.083	0.083	0.085	0.084	0.085	0.083	0.085
	0.061	0.06	0.088	0.088	0.091	0.088	0.089	0.088	0.089

Per line, the dark grey cell shows the best result (smallest RMSE value), and the light grey cell shows the second best result.

5. Conclusion

Neglecting the high order interactions between vegetation and soil background in the SAIL model, the parameters of fCover isoline in the (R, NIR) space, which are segments of straight lines, are analytical functions of the SAIL scattering parameters. Using SAIL simulations, the relationships between the fCover and the isoline slope and between the fCover and the x-coordinate of the intersection between the isoline and the soil line have been derived. These relationships allow the parametrization of the isoline set, for which the existence and the unicity of fCover solution for any (R, NIR) actual point has been demonstrated. Using a learning data set, the isoline parameter calibration was done both by Simplex and SCE–UA methods. Compared to classical vegetation indices, the method leads to better results in terms of fCover inversion and robustness against noise level. Moreover, due to its global optimization, the SCE–UA algorithm performs a little better than the Simplex method. The two limitations of the proposed method are (i) a priori knowledge (ground truth or simulated data) is needed to calibrate the 4-parameter direct model and (ii) its computation is more complex than the vegetation index method.

Next studies will then try to derive other empirical relationships between the isoline parameters and other vegetation density descriptors like the LAI or other vegetation features like the fraction of absorbed photosynthetically active radiation (FAPAR), the hot spot coefficient, ALA, C_{a+b} and N. Also heterogeneous kinds of canopy can be tested (Yoshioka et al., 2000b). In these cases, a larger number of spectral bands is required since the number of independent parameters would be higher (in particular the one-to-one relationship between LAI and fCover is no more valid). Assuming the existence of soil line between all couples of bands, a parametrization of the reflectance isolines in each plane of band couple can be adapted to solve such an inverse problem.

Acknowledgments

This work was funded by the French national programme, INSU–PNTS. The French Space Agency, CNES and the Bretagne regional direction, provide the scholarship support for this study. CNES, SPOT IMAGE, ORFEO project provided the satellite images. The authors thank W. Verhoef, M. Weiss and F. Baret for making the SAIL model available, S. Corgne and J. Nabucet for their collaboration in the constitution of the ground truth database and C. François for collaboration in the soil BRDF measurements. Sincere thanks are also extended to F. Baret for numerous constructive discussions.

Appendix A. Condition of non concurrence between three isolines

In this appendix, we show a sufficient condition of non concurrence between three different isolines.

Definition 1. *We note* $\mathcal{F}$ *the set of F line sets parameterized by* $f \in [0, 1]$. *For* $F \in \mathcal{F}$, *the corresponding line to f is called* D_f. *The slope and the intercept of* D_f *are called respectively* $\alpha(f)$ *and* $\beta(f)$. $\forall f$, $\alpha(f) \neq 0$ *and* $\alpha(f)$ *is a strictly increasing function of f.*

Property 1. $\forall f_1, f_2 \in [0, 1]$ *such that* $f_1 \neq f_2$ D_{f_1} *and* D_{f_2} *are not parallel.*

Definition 2. $F \in \mathcal{F}$, $f_1, f_2 \in [0, 1]$. M_{f_1,f_2} $(x_{f_1,f_2}, y_{f_1,f_2})$ *is the intersection between* D_{f_1} *and* D_{f_2}.

Definition 3. $M_o(x_o, y_o)$ *being a point of* $\mathbb{R}^2$ *and* $D: y = \alpha x + \beta$ *a line in* $\mathbb{R}^2$, *we say that* $M_o \in D$ *if* $y_o = \alpha x_o + \beta$, *and* $M_o \notin D$ *if* $y_o \neq \alpha x_o + \beta$.

Definition 4. $M_1(x_1, y_1)$ *and* $M_2(x_2, y_2)$ *being two points in* $\mathbb{R}^2$, *we say that* $M_2 \neq M_1$ *if* $x_2 \neq x_1$ *and* $y_1 \neq y_2$.

Property 2. *Let* $F \in \mathcal{F}$, $D_f \in F$ *and* $M_1(x_1, y_1)$, $M_2(x_2, y_2) \in D_f$. $x_2 \neq x_1 \Leftrightarrow y_2 \neq y_1 \Leftrightarrow M_2 \neq M_1$. *(Proof: use* $\alpha(f) \neq 0$*)*

Definition 5. *We say that* $F \in \mathcal{F}$ *verifies the increasing property, noted* $F\nearrow$, *if* $\forall f_0, f_1, f_2 \in [0, 1]$ *such that* $f_0 < f_1 < f_2$, $M_{f_0,f_1} < M_{f_0,f_2}$.

Fig. A.1. *shows such a configuration:* $M_{f_0,f_1} < M_{f_0,f_2} < M_{f_0,f_3}$ *and* $M_{f_1,f_2} < M_{f_1,f_3}$.

Definition 6. *We say that* $F \in \mathcal{F}$ *verifies the increasing property restrictively to the interval [a, b], noted* $F\nearrow_{[a,b]}$, *if* $\forall f_0, f_1, f_2 \in [a, b]$ *such that* $f_0 < f_1 < f_2$, $M_{f_0,f_1} < M_{f_0,f_2}$.

Property 3. *Let* $F \in \mathcal{F}$. $F\nearrow_{[a,b]} \Leftrightarrow \forall f_0, f_1, f_2 \in [a, b] / f_0 < f_1 < f_2$, $M_{f_0,f_1} < M_{f_0,f_2} \Leftrightarrow r_{f_0,f_1} < r_{f_1,f_2} \Leftrightarrow \frac{y_{f_1,f_2} - y_{f_0,f_2}}{x_{f_1,f_2} - x_{f_0,f_2}} < \frac{y_{f_1,f_2} - y_{f_0,f_1}}{x_{f_1,f_2} - x_{f_0,f_1}}$.

Property 4. *Let* $F \in \mathcal{F}$ *and* $a, b \in [0, 1]$, *such that* $a < b$. *If* $F\nearrow_{[a,b]}$, *then* $\forall f_0, f_1, f_2 \in [a, b]$, *such that* $f_0 \neq f_1$, $f_1 \neq f_2$ *and* $f_2 \neq f_0$, $D_{f_0} \cap D_{f_1} \cap D_{f_2} = \emptyset$.

Property 5. $F \in \mathcal{F}$, $f_0, f_1, f_3 \in [0, 1]$, *such that* $f_0 < f_1 < f_2$, $A \in D_{f_1}$. *Then,* $A \neq D_{f_0} \Leftrightarrow A \neq M_{f_0,f_1}$ *and* $A \neq D_{f_2} \Leftrightarrow A < M_{f_1,f_2}$ *(Fig. A.1 illustrates the A configuration relative to* D_{f_0} *and* D_{f_2}*).*

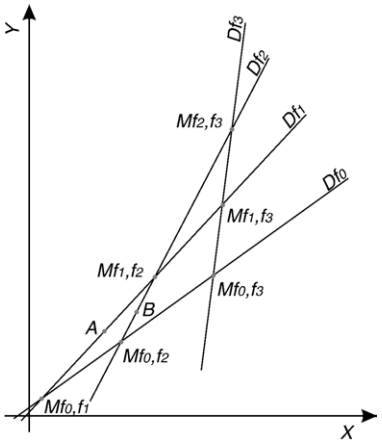

Lemma 1. $F \in \mathcal{F}$, $f_0, f_1, f_2 \in [0, 1]$, *such that* $f_0 < f_1 < f_2$. *If* $M_{f_0,f_2} \neq M_{f_0,f_1}$ *then* $M_{f_1,f_2} \neq D_{f_0}$, $M_{f_1,f_2} \neq M_{f_0,f_1}$ *and* $M_{f_1,f_2} \neq M_{f_0,f_2}$. *Reciprocally, if* $M_{f_1,f_2} \neq D_{f_0}$, *then* $M_{f_0,f_2} \neq M_{f_0,f_1}$.

Proof. *direct sense* $\Rightarrow$ Let $A \in D_{f_1}$ and $B \in D_{f_2}$ such that $A \neq D_{f_0}$ and $B \neq D_{f_0}$ (cf. Fig. A.1):

$$\widehat{(AM_{f_0;f_1}; BM_{f_0;f_2}} < \widehat{(AM_{f_0;f_1}; M_{f_0;f_1}M_{f_0;f_2}} < \widehat{(M_{f_0;f_1}M_{f_0;f_2}; BM_{f_0;f_2}} < 2k];$$
$$\text{or } \widehat{(M_{f_0;f_1}A; M_{f_0;f_1}M_{f_0;f_2}} < \widehat{(M_{f_0;f_1}M_{f_0;f_2}; M_{f_0;f_2}B} < 2k];$$
$$\text{or } \widehat{(M_{f_0;f_1}M_{f_0;f_2}; AB} < \widehat{(M_{f_0;f_1}M_{f_0;f_2}; M_{f_0;f_2}B} < 2k].$$

Since $(M_{f_0,f_2}M_{f_0,f_2})$, $(M_{f_0,f_1}A)$ and $(M_{f_0,f_2}B)$ are respectively collinear to D_{f_0}, and D_{f_1}, and D_{f_2} and $\alpha(f)$ is an increasing function of f, then $\pi - \widehat{BM_{f_0;f_2}M_{f_0;f_1}} \neq \widehat{AM_{f_0;f_1}M_{f_0;f_2}}$:

$$2k < \widehat{(M_{f_0;f_1}M_{f_0;f_2}; M_{f_0;f_1}A} < \widehat{(M_{f_0;f_1}M_{f_0;f_2}; M_{f_0;f_2}B} < 2k.$$

Then, $2k < \widehat{(AM_{f_0;f_1}; BM_{f_0;f_2}} < 2k$. Therefore the intersection between (AM_{f_0,f_1}) and (BM_{f_0,f_2}) is situated in the half plan above D_{f_0}: $M_{f_1,f_2} \neq D_{f_0}$ (see Fig. A.1).

Now; $M_{f_1;f_2} \in D_{f_1}$ $\Rightarrow$ $M_{f_1;f_2} \neq M_{f_0;f_1}$:
$M_{f_1;f_2} \neq D_{f_0}$ $\Rightarrow$ $f_0 < f_1$ *P*:5

By the same way, we obtain $M_{f_1,f_2} \neq M_{f_0,f_2}$.

reciprocal sense $\Leftarrow$

$M_{f_1;f_2} \in D_{f_1}$ $\Rightarrow$ $f_0 < f_1 \Rightarrow f_0 < f_2$ $\Rightarrow$ $M_{f_0;f_1} \neq M_{f_0;f_2}$
$M_{f_1;f_2} \neq D_{f_0}$ $\Rightarrow$ *P*:5 $M \neq M$

$\Rightarrow$ *P*:5 $M_{f_0;f_1} \neq D_{f_2} \Rightarrow M_{f_0;f_1} \in D_{f_0}$ $\Rightarrow$ $f_0 < f_2 \Rightarrow M_{f_0;f_1} \neq M_{f_0;f_2}$: □
$M_{f_0;f_1} \neq D_{f_2}$ $\Rightarrow$ *P*:5 M

Lemma 2. $F \in \mathcal{F}$, $f_0, f_1, f_2, f_3 \in [0, 1]$ *and* D_{f_0}, *such that* $f_0 < f_1 < f_2 < f_3$. *If* $M_{f_0,f_2} \neq M_{f_0,f_1}$, *and* $M_{f_1,f_3} \neq M_{f_1,f_2}$ *then* $M_{f_0,f_3} \neq M_{f_0,f_2}$ *(cf.* Fig. A.1*).*

Proof

$M_{f;f} \neq M_{f;f}$ $\Rightarrow$ *L*:1 $M_{f_1;f_2} \neq M_{f_0;f_2}$

$M_{f_2;f_3} \neq M$ $\Rightarrow$ $f_0 \neq D_f$ $\Rightarrow$ $f_0; f_3$ $f_0; f_2$

Z $M_{f_2;\,f_3}$ N$M_{f_0;\,f_2}$

N$M_{f_1;\,f_2}$

2 $f_2;f_3$

$f_0;f_2$ 2 3 0

f_1bf_2bf_3 L:1 $f_2;f_3$ 0 2 0 1

$M_{f\ ;f}$ N$M_{f\ ;f}$ Z M

1 3 1 2

$f_1 \mathrm{b} f_2$

$$f\,\mathsf{a}D_f \quad \mathsf{g}^{P:5} M \quad \mathsf{N}D \qquad f_0\mathsf{b}f_2\mathsf{b}f_3 \quad \mathsf{g}^{L:1r} M \quad \mathsf{N}M \qquad \square$$

$A \in D_f$ and $B \in D_f$ such that $A \cap D_f$ and $B \cap D_f$.

1] such as $f_{22} \neq f_{33}$. *If* $M_{f,f} \neq M_{f,f} \neq M_{f,f}$ *then* $M_{f,f} \neq M_{f,f}$.

Proof

Proof. *Let* $n \in N^*$, *such that* $n \geq 1$, $\forall i \in \{1 \ldots 2n-1\}$ $a_i = \frac{i-1}{2n}$ and $b_i = \frac{i+1}{2n}$.

Lemma 4. *Let* $F \in \mathcal{F}$ *and* $a, b \in [0, 1]$, *such that* $a \leq b$, α *and* β *(see Definition 1) are* C^1 *functions. Then* $F \nearrow$ *if* $\forall f, f \in [a, b]$

$\square$

$$\begin{cases} \\ \\ \end{cases}$$

$$\begin{cases} \\ \end{cases}$$

$$P:5$$

$$L:1r$$

$$i \qquad i \qquad \mathbb{k}a_i;b_i]$$

Theorem 2 (The increasing property). *Let F*aF*, such that* α*,* β *are* C^2 *functions, and* α‴ *and* β‴ *exist. Then F*↗ *if* ∀*f*∈[0, 1]:

bWaV— bVaW b0:

{z }
w

2

2

b —e þ e *A;*

$$M_{f_{00};f_1} \mathrm{b} M_{f_{00};f_2} \eth F \subset_{\Vdash} f_0; f_2] \mathrm{b} \quad \mathsf{Z}\, M_{f_{00};f_2} \mathrm{b} M_{f_{00};f_{22}} \quad \mathsf{Z} M_{f_{00};f_{11}} \mathrm{b} M_{f_{00};f_{22}}$$
$$\tfrac{1}{2}_{1};\ {}_{3}] \mathrm{b}$$
$$M_{f_{00};\, f_{11}} \mathrm{b} M_{f_{00};\, f_2} \eth F \subset_{\Vdash} f_0;\, f_2] \mathrm{b}$$

- case 3: $f \leq f \quad \underline{f} \quad f \quad f \quad f \leq f$:

g

00 22 00 11 00 22

00 1 00 2 0 2 g

$$d\,\frac{b\delta f_1 \flat - b\delta f_0 \flat}{}$$

0 1 2 3 0 1 2 aðƒiÞ—aðƒiÞ b0: ðA:1Þ

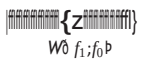

$_{00}, f_{11}$ $_{00}, f_{22}$

Proof. $\Psi(f^1, f^0) \geq 0$ then $\frac{\partial f_1}{\partial f} - \frac{\partial f_0}{\partial f}$ is a strictly increasing

show that M_f $\geq M_f$ in any of the six cases:

0 2

$$-\left(a(f)-a(f)\right)^{b-}\left(a(f)-a(f)\right)^{Z}F\subset_{[a;b]}:$$

$$M_{f_1,f_2} \mathrm{b} M_{f_1,f_{22}} \eth F \subset {}_{f} {}_{f}$$

$$0 \quad {}_{00}b \; {}_{1}b \; {}_{11}b \; {}_{2}b \; {}_{22} \quad 3$$

$\psi(f) \geq 0$. Then $a \in \mathbb{R}^*$, such that $\psi \geq -\varepsilon$.

$f_{00} \le f_{11} \le f_2 \le f_{22}$
$M_{f_{00};\, f_{11}} \subset M_{f_{00};\, f_2} \subset F[f_0;\, f_2]$
$M_{f_{11};\, f_2} \subset M_{f_{11};\, f_{22}} \subset F[f_1;\, f_3]$

Let $f_0, f_1 \in [0, 1]$, such that $f_0 \le f_1$:

(1) $\forall f_1 \ge f_0$ and $\forall f_1 > f_0$, $M_{f_1} \subset M_{f_0}$;

(2) $\forall f_1 > f_0$, $M_{f_1} \subset M_{f_0}$ with $\dim(M_{f_1}) < \dim(M_{f_0})$;

L:2

$Z = M_{f_{00};f_{11}} \cup M_{f_{00};f_{22}}$

$M_{f_{00},f} \Rightarrow M_{f_{00},f} \cup M_{f_{11},f}$

- case 4: $f_0 \le f_{00} \le f_1 \le f_{11} = f_2$

f_{00}, f_2 b

b $f_{22} \leq f_3$: as in case 2, M

(wð f_0Þþ Oð f_1 — f_0Þb0;

where O verifies: $\underline{\rho}$aAaRÞ=8f a⁄0; 1]; Oð f ÞbfA

)

$M_{f\ ;f}$ bM_f

f_{00} bf_{11} bf_{22}

$;f$ ðF ⊂ $f\ ;f\ ]$þ *L*:3

Z $M_{f_{00};f_{11}}$ b$M_{f_{00};f_{22}}$

$$w\eth f_0 \flat \quad O \quad \eth f_1 \quad -f_0 \flat \quad \mathrm{b} - e \flat \eth f_1 - f_0 \flat A;$$

$M_{f_1;f_2} \flat M_{f_1;f_{11}} \flat M_{f_1;f_{22}} \eth F \subset_{\natural f_1;f_3]} \flat$ $\flat$

• case 6: $f_0 \flat f_1 \leq f_{00} \flat f_{11} \flat f_{22} \leq f_3$: then f_{00}, f_{11}, $f_{22} \in [f_1, f_3]$, $F\nearrow[f_1, f_3]$ by assumption. □

Proposition 1. *Let* $F \mathsf{a} \mathsf{F}; n \mathsf{a} N^*$, $a_1, \ldots, a_n, b_1, \ldots, b_n \in [0, 1]$ *such that* $0 = a_1 \leq a_2 \flat b_1 \leq a_3 \flat b_2 \leq a_4 \flat b_3 \leq a_5 \ldots a_{n-1} \flat b_{n-2} \leq a_n \flat b_{n-1} \leq b_n = 1$. *If* $\forall i \in \{1, \ldots, n\}$, $F\nearrow_{[a_i, b_i]}$, *then* $F\nearrow$.

Proof. Use the Theorem 1 and a recurrence over the total number of intervals n. □

Proposition 2. *Let* $F \mathsf{a} \mathsf{F}$. *If* $\exists \varepsilon \mathsf{N} 0$ *such that* $\forall f \in [0, 1]\ F\nearrow_{[f, f+\varepsilon]}$, *then* $F\nearrow$.

0 :

Then, $\forall f_0, f_1 \in [f, f+\varepsilon_0] / f_0 \flat f_1$, $\Psi(f_1, f_0) \flat 0$. Then, $\forall f \in [0, 1]$ $F\nearrow[f, f+\varepsilon_0]$. Therefore, according to the Proposition 2 $F\nearrow$. □

References

Anderson, J. A. (1995). *An introduction to neural networks.* Cambridge, MA: MIT Press.

Andrieu, B., Baret, F., Jacquemoud, S., Malthus, T., & Steven, M. (1997). Evaluation of an improved version model for simulating bidirectional of sugar beet canopies. *Remote Sensing of Environment*, *60*, 247−257.

Baret, F., & Buis, S. (2007). Estimating canopy characteristics from remote sensing observations. *Review of methods and associated problems* : Springer.

Baret, F., Clever, J. G. P. W., & Steven, M. D. (1995). The robustness of canopy gap fraction estimates from red and near infrared reflectances: A comparison of approaches. *Remote Sensing of Environment*, *54*, 141−151.

Baret, F., & Guyot, G. (1991). Potentials and limits of vegetation indices for lai and apar assessment. *Remote Sensing of Environment*, *35*(2–3), 161–173.

Baret, F., Guyot, G., & Major, D. (1989). Tsavi: A vegetation index which minimizes soil brightness effects on lai and apar estimation. *12th Canadian symposium on remote sensing and IGARSS'90, Vol. 4* (pp.1355–1359): IEEE.

Baret, F., Jacquemoud, S., & Hanocq, J. F. (1993). The soil line concept in remote sensing. *Remote Sensing Reviews*, *7*, 65–82.

Campbell, G. S. (1990). Derivation of an angle density function for canopies with ellipsoidal leaf angle distribution. *Agricultural and Forest Meteorology*, *49*, 173–176.

Clevers, J. G. P. W. (1989). The application of a weighted infrared–red vegetation index for estimation leaf area index by correcting for soil moisture. *Remote Sensing of Environment*, *25*, 53–69.

Combal, B., Baret, F., Weiss, M., Trubuil, A., Macé, D., Pragnère, A., et al. (2002). Retrieval of canopy biophysical variables from bidirectional reflectance using prior information to solve the ill-posed inverse problem. *Remote Sensing of Environment*, *84*, 1–15.

Cooper, K., Smith, J. A., & Pitts, D. (1982). Reflectance of a vegetation canopy using the adding method. *Applied Optics*, *21*(22), 4112–4118.

Corgne, S., Hubert-Moy, L., Barbier, J., Mercier, G., & Solaiman, B. (2002). Follow-up and modelling of the land use in an intensive agricultural watershed in France. In L. Toulios (Ed.), *Remote sensing for agriculture, ecosystems, and hydrology IV, Vol. 4879* (pp.342–351) Manfred Owe: SPIE.

Dabney, S., Delgado, J., & Reeves, D. (2001). Using winter crops to improve soil and water quality. *Communication in Soil Science Plant Annals*, *32*(7–8), 1221–1250.

Dantzig, G., Orden, A., & Wolfe, P. (1955). The generalized simplex method for minimizing a linear form under inequality restraints. *Pacific Journal of Mathematics*, *8*, 183–195.

Duan, Q., Sorooshian, S., & Gupta, V. K. (1992). Effective and efficient global optimization for conceptual rainfall-runoff models. *Water Resources Research*, *28*(4), 1015–1031.

Durand, P., Beaujouan, V., Ruiz, L., Aurousseau, P., & Cotteret, G. (2002). A hydrological model dedicated to topography-based simulation of nitrogen transfer and transformation: rationale and application to the geomorphology–denitrification relationship. *Hydrological Processes*, *16*(2), 493–507.

Fourty, T., & Baret, F. (1997). Vegetation water and dry matter contents estimated from top-of-the atmosphere reflectance data: A simulation study. *Remote Sensing of Environment*, *61*, 34–45.

Fourty, T., & Baret, F. (1998). On spectral estimates of fresh leaf biochemistry. *International Journal of Remote Sensing*, *19*, 1283–1297.

Gausman, H. W., Allen, W. A., Cardenas, R., & Richardson, A. J. (1970). Relationship of light reflectance to histological and physical evaluation of cotton leaf maturity. *Applied Optics*, *9*(3), 545–552.

Holben, B., & Kimes, D. (1986). Directional reflectance response in avhrr red and near-ir bands for three cover types and varying atmospheric conditions. *Remote Sensing of Environment*, *19*, 213–236.

Huete, A. R. (1988). A soil-adjusted vegetation index (savi). *Remote Sensing of Environment*, *25*, 295–309.

Huete, A. R. (1989). *Theory and applications of optical remote sensingCh. Soil influences in remotely sensed vegetation–canopy spectra*. (pp. 107–141) New York: John Wiley & Sons.

Huete, A. R., Post, D., & Jackson, R. D. (1984). Soil spectral effects on 4-space vegetation discrimination. *Remote Sensing of Environment*, *15*, 155–165.

Jacquemoud, S., & Baret, F. (1990). Prospect: A model of leaf optical properties spectra. *Remote Sensing of Environment*, *34*(2), 75–91.

Kimes, D. S., Knyazikhin, Y., Privette, J. L., Abuelgasim, A. A., & Gao, F. (2000). Inversion methods for physically-based models. *Remote Sensing Reviews*, *18*, 381–439.

Kuusk, A. (1985). The hot spot effect of a uniform vegetative cover. *Sovietic Journal of Remote Sensing*, *3*(4), 645–658.

Kuusk, A. (1991). Determination of vegetation canopy parameters from optical measurements. *Remote Sensing of Environment*, *37*, 207–218.

Kuusk, A. (1991). Photon–vegetation interactions. Applications in optical remote sensing and plant ecology. *Ch. The hot spot e1ect in plant canopy reflectance* (pp. 139–159). Berlin: Springer.

Kuusk, A. (1995). A fast, invertible canopy reflectance model. *Remote Sensing of Environment*, *51*, 342–350.

Nelder, J., & Mead, R. (1965). A simplex method for function minimization. *Computer Journal*, *7*, 308–313.

Nilson, T. (1971). A theoretical analysis of the frequency of gaps in plant stands. *Agricultural Meteorology*, *8*, 25–38.

Pearson, R. L., Miller, L. D., 1972. Remote mapping of standing crop biomass for estimation of the productivity of the short grass prairie. In: ERIM, Ann Arbor, M. (Ed.), 8th international symposium on remote sensing of the environment. Pawnee National Grasslands, Colorado, pp. 1357–1381.

Qi, J., Chehbouni, A., Huete, A. R., & Kerr, Y. H. (1994). A modified soil adjusted vegetation index. *Remote Sensing of Environment*, *48*, 119–126.

Richardson, A. J., & Wiegand, C. L. (1977). Distinguishing vegetation from soil background information. *Photogrammetric Engineering Remote Sensing*, *43*, 1541–1552.

Rondeaux, G., Steven, M., & Baret, F. (1996). Optimisation of soil-adjusted vegetation indices. *Remote Sensing of Environment*, *55*, 95–107.

Rouse, J. W., Haas, R. H., Schell, J. A., Deering, D. W., & Harlan, J. C. (1974). Monitoring the vernal advancement retrogradation of natural vegetation. *NASA/GSFC, Vol. 3*.

Rumelhart, D., Hinton, G., Williams, R., 1986. Learning internal representations by error propagation. In: D. Rumelhart, J.M., the PDP research group (Eds.), Parallel Distributed Processing: Explorations in the microstructure of cognition. Vol. 1. Foundations, MIT Press, Cambridge, MA, pp. 318–362.

Sorooshian, S., Duan, Q., & Gupta, V. K. (1992). Calibration of the sma–nwsrfs conceptual rainfall-runoff model using global optimization. *Water Resources Research*, *29*(4), 1185–1194.

Suits, G. H. (1972). The calculation of the directional reflectance of a vegetative canopy. *Remote Sensing of Environment*, *2*, 117–125.

Tanré, D., Deroo, C., Duhaut, P., Herman, M., & Morcrette, J. (1990). Description of a computer code to simulate the satellite signal in the solar spectrum: The 5s code. *International Journal of Remote Sensing*, *11*(4), 659–668.

van de Hulst, H. C. (1981). *Light scattering by small particles.* New York: Dover Publications, Inc.

Verhoef, W. (1984). Light scattering by leaf layers with application to canopy reflectance modelling: The sail model. *Remote Sensing of Environment*, *16*, 125–141.

Verhoef, W. (1985). Earth observation modeling based on layer scattering matrices. *Remote Sensing of Environment*, *17*, 165–178.

Vermote, E., Tanré, D., Deuzé, J., Herman, M., & Morcette, J. (1997). Second simulation of the satellite signal in the solar spectrum, 6s: An overview. *IEEE Transactions on Geoscience and Remote Sensing*, *35*(3), 675–686.

Verstraete, M. M., Pinty, B., & Dickinson, R. E. (1990). A physical model of the bidirectional reflectance of vegetation canopies, part 2: Inversion and validation. *Journal of Geophysical Research*, *95*, 11767–11775.

Yoshioka, H. (2004). Vegetation isoline equations for an atmosphere–canopy–soil system. *IEEE Transactions on Geoscience and Remote Sensing*, *42*, 166–175.

Yoshioka, H., Huete, A. R., & Miura, T. (2000). Derivation of vegetation isoline equations in red–nir reflectance space. *IEEE Transactions on Geoscience and Remote Sensing*, *38*(2), 838–848.

Yoshioka, H., Miura, T., & Huete, A. R. (2003). An isoline-based translation technique of spectral vegetation index using eo-1 hyperion data. *IEEE Transactions on Geoscience and Remote Sensing*, *41*, 1363–1372.

Yoshioka, H., Miura, T., Huete, A. R., & Ganapol, B. D. (2000). Analysis of vegetation isolines in red–nir reflectance space. *Remote Sensing of Environment*, *74*(2), 313–326.

Yoshioka, H., Yamamoto, H., & Miura, T. (2002). Use of an isoline-based inversion technique to retrieve a leaf area index for inter-sensor calibration of spectral vegetation index. *Geoscience and Remote Sensing Symposium, Vol. 3* (pp.1639–1641): IGARSS.